Inorganic Chemistry

Article

pubs.acs.org/IC

Synthesis, Structure, and Properties of Two Zintl Phases around the Composition SrLiAs

Xian-Juan Feng,[†,‡,§] Yurii Prots,[‡] Marcus Peter Schmidt,[‡] Stefan Hoffmann,[‡] Igor Veremchuk,[‡] Walter Schnelle,[‡] Ulrich Burkhardt,[‡] Jing-Tai Zhao,[†] and Yuri Grin*[,‡]

[†]Key Laboratory of Transparent Opto-Functional Inorganic Materials of Chinese Academy of Sciences, Shanghai Institute of Ceramics, Shanghai 200050, China

[‡]Max-Planck-Institut für Chemische Physik fester Stoffe, Nöthnitzer Strasse 40, 01187 Dresden, Germany

[§]University of Chinese Academy of Science, Beijing 100080, China

Supporting Information

ABSTRACT: Two atomic arrangements were found near the equiatomic composition in the strontium−lithium−arsenic system. Orthorhombic *o*-SrLiAs was synthesized by reaction of elemental components at 950 °C, followed by annealing at 800 °C and subsequent quenching in water. The hexagonal modification *h*-$SrLi_{1-x}As$ was obtained from annealing of *o*-SrLiAs at 550 °C in dynamic vacuum. The structures of both phases were determined by single-crystal X-ray diffraction: *o*-SrLiAs, structure type TiNiSi, space group *Pnma*, Pearson symbol *oP*12, a = 7.6458(2) Å, b = 4.5158(1) Å, c = 8.0403(3) Å, V = 277.61(2) Å^3, R_F = 0.028 for 558 reflections; *h*-$SrLi_{1-x}As$, structure type ZrBeSi, space group $P6_3/mmc$, Pearson symbol *hP*6, a = 4.49277(9) Å, c = 8.0970(3) Å, V = 141.54(1) Å^3, R_F = 0.026 for 113 reflections. The analysis of the electron density within the framework of the quantum theory of atoms in molecules revealed a charge transfer according to the $Sr^{1.3+}Li^{0.8+}As^{2.1-}$, in agreement with the electronegativities of the individual elements. The electron localizability indicator distribution indicated the formation of a 3D anionic framework [LiAs] in *o*-SrLiAs and a rather 2D anionic framework [LiAs] in *h*-$SrLi_{1-x}As$. Magnetic susceptibility measurements point to a diamagnetic character of both phases, which verifies the calculated electronic density of states.

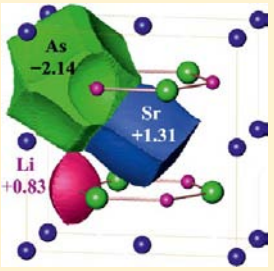

1. INTRODUCTION

A large number of ternary compounds with the equiatomic composition ABX have been reported in past decades, where A is alkali, alkaline-earth, or rare-earth metals, B represents transition metals or Li, and X is an element of group 14 or 15.[1−3] Formed by electropositive elements and the elements at the Zintl border such as Sn and Sb, ABX compounds display a large variety of structure types and physical properties.[4,5] Some of them could be described as Zintl phases, e.g., $A^{2+}Li^{+}Sb^{3-}$ (A = Ca, Sr, Ba).[6−8] The lithium-containing compounds ALiAs, ALiSb, ALiBi were synthesized with A = Eu, Yb, Ca, Sr, Ba (Table 1).[9] They crystallize either in the orthorhombic structure type TiNiSi (space group *Pnma*) or in the hexagonal structure type ZrBeSi (space group $P6_3/mmc$). Conspicuous for the ALiAs series is that the strontium representatives were not reported so far. The present investigation is dedicated to the synthesis and physical properties of two hitherto unknown phases around the composition SrLiAs. Preliminary results of this work were presented at a conference.[10]

Table 1. Crystal Structures of the Compounds ALiX

	X		
A	As	Sb	Bi
Ca	TiNiSi[9]	TiNiSi[7]	TiNiSi[9]
Sr		TiNiSi[9]	TiNiSi[9]
Ba	SrPtSb[9]	ZrBeSi[9]	
Eu	TiNiSi[5]	TiNiSi[2]	TiNiSi[2]
Yb	TiNiSi[9]	TiNiSi[9]	TiNiSi[9,a]

[a]YbLiBi was previously reported to crystallize in YbLiBi type, space group $P6_3mc$.[2]

2. EXPERIMENTAL SECTION

2.1. Synthesis. Orthorhombic *o*-SrLiAs was synthesized from its constituting elements: strontium (99.95%, Alfa Aesar), lithium (99.9%, Alfa Aesar), and arsenic (99.999%, Alfa Aesar). The starting mixtures were loaded into tantalum tubes, which were arc-welded and then jacketed by quartz ampules. The whole packages were heated to 950 °C within 12 h and left to react at this temperature for 6 h. After a subsequent annealing at 800 °C for 96 h, the samples were quenched in water. If the starting mixture was heated to above 1000 °C, a reaction with the crucible was observed; the byproduct was identified as $TaSr_3Li_7As_6$.[11] Single-phase hexagonal *h*-$SrLi_{1-x}As$ was obtained by annealing *o*-SrLiAs at 550 °C in a tungsten crucible under dynamic vacuum of 10^{-3} mbar in a quartz tube for 2 h. In order to avoid the reaction of quartz with the evaporated lithium, the tungsten crucible was isolated by an additional steel jacket. Due to the sensitivity of the starting materials as well as the products against moisture and oxygen, all handlings were performed in a glovebox filled with purified argon (MBraun, H_2O < 1 ppm; O_2 < 1 ppm).

Received: May 10, 2013
Published: July 17, 2013

   dx.doi.org/10.1021/ic401166v | *Inorg. Chem.* 2013, 52, 8971−8978

2.2. Powder X-ray Diffraction. The powder X-ray diffraction patterns of the *o*-SrLiAs and *h*-$SrLi_{1-x}As$ samples were recorded utilizing a Huber imaging plate Guinier camera G670 (Cu $K\alpha_1$ radiation λ = 1.540 56 Å, 2θ interval of 4−100°, exposure time 6 × 15 min). The powder diffraction data were evaluated with the WinXPow package.[12] Lattice parameters of both phases were refined by least-squares fittings of Guinier powder diffraction data using LaB_6 (a = 4.156 92 Å) as internal standard. The WinCSD program package was used for profile fitting and lattice parameter determination.[13]

2.3. Crystal Structure Determination. The crystal structures of *o*-SrLiAs and *h*-$SrLi_{1-x}As$ were investigated using single-crystal X-ray diffraction. Irregularly shaped single crystals separated from the samples after heat treatments were fixed with glue and enclosed by glass capillaries filled with argon. The diffraction data were collected using Rigaku AFC7 diffractometer equipped with a Saturn 724+ CCD detector (monochromatic Mo Kα radiation, λ = 0.710 73 Å). The intensities of the measured reflections were corrected for absorption using the multiscan technique.[14]

Crystal structure refinements were performed by full-matrix least-squares on F within the program package WinCSD.[13] Both structure models were standardized by the STRUCTURE TIDY program.[15]

2.4. Thermal Analysis. Thermochemical properties of *o*-SrLiAs and *h*-$SrLi_{1-x}As$ were investigated by thermal gravimetry (TG) and differential scanning calorimetry (DSC) employing the Netzsch STA 449C calorimetric setup. The measurements were performed with a heating rate of 10 K/min between room temperature and 1100 °C. The results discussed below were obtained on samples put into BN crucibles either with a small hole on the cap or open. After each experiment, the samples were characterized by powder X-ray diffraction.

2.5. Chemical Composition and Microstructure Analysis. Chemical analysis with respect to constituent elements (Sr, Li, and As) as well as to oxygen and other possible contaminations were performed on samples containing mainly phases *o*-SrLiAs and *h*-$SrLi_{1-x}As$. The oxygen analysis was conducted using a Leco TCH 600 analyzer. The mass of the individual sample was approximately 5 mg, which corresponds according to the detection limit of oxygen to 0.25 mass %. Weighed powders were put into tin capsules under argon and transferred into the graphite die of the analyzer. The contents of the majority components were determined by using inductively coupled plasma optical emission spectrometry (ICP-OES) on a Varian VISTA RL spectrometer. Samples were placed into Teflon container for each experiment. The resulting values are averages over three measurements in each case.

A metallographic study was executed on an *o*-SrLiAs bulk sample polished under Ar using hexane as a lubricant. The microstructure of the sample was analyzed using both a light-optical microscope (Zeiss Axioplan2) and a scanning electron microscope (Cameca SX100 microprobe with W-cathode). The constituent elements were confirmed by energy dispersive X-ray spectroscopy (EDX, EDAX) on a scanning electron microscopy with an attached Sr (Li)-detector. Phase compositions were evaluated by wavelength-dispersive X-ray spectroscopy on an electron microprobe (WDXS, Cameca SX100, W cathode). The intensities of X-ray lines Sr Lα and As Lα were used to calculate the local chemical composition; $SrGa_4$ (Sr Lα: 155.6 cps/nA) and ZrAsSe (As Kα: 380.4 cps/nA) were used as references to evaluate elemental mass fractions for Sr and As, respectively. A beam current of 30 nA led to count rates of about 10 kcps on spectrometers with TAP and LiF crystals with the statistic deviations of no more than 0.31 mass %. Applying the $\varphi(\rho z)$-matrix correction model, the atomic fractions and their accuracies were calculated from the measured X-ray intensities by averaging mass fraction values from 10 different locations on each sample. The mass fraction of Li was determined by difference.

2.6. Physical Property Measurements. In order to measure physical properties, the powdered samples of containing mainly *o*-SrLiAs or *h*-$SrLi_{1-x}As$ phases were compacted into bars (1.5 × 1.5 × 8 mm^3) using a tungsten carbide die by spark plasma sintering (SPS). The experimental conditions were optimized by variation of the sintering temperature and applied pressure. A temperature of 200 °C and a pressure of 580 MPa were found as optimum conditions. Deviations from these parameters resulted in fragile bars. The phase purity of the so-obtained bars was proven by powder X-ray diffraction before the physical properties measurement. Parts of the compacted samples of *o*-SrLiAs and *h*-$SrLi_{1-x}As$ were sealed into quartz tubes under 0.4 bar of helium to protect the samples from the influence of temperature and humidity during the magnetic measurements. The magnetization measurements were performed in external magnetic fields $\mu_0 H$ ranging from 10 mT to 7 T to between 1.8 and 400 K using a SQUID magnetometer (MPMS-XL7, Quantum Design). The signals of the empty sample holders were subtracted.

2.7. Calculation Procedure. Electronic structure calculation and analysis of chemical bonding were carried out for the completely occupied models for both phases, i.e., *o*-SrLiAs and *h*-$SrLi_{1-x}As$ with x = 0, with the respective lattice parameters and atomic positions obtained from the single-crystal X-ray refinement reported in this study (Tables 2 and 3). For *h*-$SrLi_{1-x}As$, only the ideal positions of As atoms at ($^1/_3$, $^2/_3$, $^1/_4$) were considered. The TB-LMTO-ASA program package was employed.[16] The Barth−Hedin exchange potential[17] was used for the LDA calculations. The radial scalar-relativistic Dirac equation was solved to obtain the partial waves. Because the calculation within the atomic sphere approximation (ASA) includes corrections for the neglect of interstitial regions and partial waves of higher order,[18] an addition of empty spheres was not necessary. The following radii of the atomic spheres were applied for the calculations: r(Sr) = 1.948 Å, r(Li) = 1.425 Å, and r(As) = 1.758 Å for *o*-SrLiAs; r(Sr) = 2.142 Å, r(Li) = 1.334 Å, and r(As) = 1.674 Å for *h*-$SrLi_{1-x}As$ (x = 0). For each calculation, a basis set containing Sr(5s, 4d), Li(2s), and As(4s, 4p) orbitals was employed with Sr(5p, 4f), Li(2p, 3d), and As(4d) functions being down-folded.

Table 2. Crystallographic Data for *o*-SrLiAs and *h*-$SrLi_{1-x}As$

	o-SrLiAs	*h*-$SrLi_{1-x}As$
T	295 K	295 K
crystal size	0.080 × 0.100 × 0.100 mm^3	0.085 × 0.100 × 0.110 mm^3
crystal system	orthorhombic	hexagonal
space group	*Pnma*	$P6_3/mmc$
unit cell dimensions[a]		
a	7.6458(2) Å	4.49277(9) Å
b	4.5158(1) Å	
c	8.0403(3) Å	8.0970(3) Å
unit cell volume, Z	277.61(2) $Å^3$, 4	141.54(1) $Å^3$, 2
density (calcd)	4.06 g/cm^3	3.94 g/cm^3
F(000)	296	146.5
diffractometer	Rigaku AFC 7	Rigaku AFC 7
detector	Saturn 724+	Saturn 724+
radiation, wavelength	Mo Kα, 0.710 73 Å	Mo Kα, 0.710 73 Å
abs coeff	30.87 mm^{-1}	30.04 mm^{-1}
θ range for data collection	2.53−34.39	2.50−33.40
index ranges	$-11 \le h \le 11$	$-6 \le h \le 4$
	$-5 \le k \le 6$	$-6 \le k \le 6$
	$-12 \le l \le 11$	$-12 \le l \le 9$
reflns collected	2737	1133
indep reflns	615	130
R(int)	0.037	0.039
obsd reflns [$I > 2\sigma(I)$]	558	113
extinction coefficient	0.0097(6)	0.036(4)
refinement method	full-matrix least-squares on F	full-matrix least-squares on F
R_F	0.028	0.026
largest diff hole, peak	−1.01, 1.21 $e/Å^3$	−1.07, 1.31 $e/Å^3$

[a]Obtained from powder X-ray diffraction data.

dx.doi.org/10.1021/ic401166v | *Inorg. Chem.* 2013, 52, 8971−8978

Table 3. Atomic Coordinates and Displacement Parameters for *o*-SrLiAs and *h*-SrLi$_{1-x}$As

atom	Wyckoff site	*x*	*y*	*z*	*B* (is/eq)
o-SrLiAs					
Sr	4*c*	0.0064(1)	$^1/_4$	0.7064(1)	0.90 (1)
Li	4*c*	0.157(2)	$^1/_4$	0.074(2)	1.6(3)
As	4*c*	0.2750(1)	$^1/_4$	0.4062(1)	0.77(1)
h-SrLi$_{1-x}$As					
Sr	2*a*	0	0	0	1.07(2)
Li[a]	2*d*	$^1/_3$	$^2/_3$	$^3/_4$	0.83(5)
As1[a]	2*c*	$^1/_3$	$^2/_3$	$^1/_4$	0.68(2)
As2[a]	4*f*	$^1/_3$	$^2/_3$	0.280(1)	0.67(5)

atom	B_{11}	B_{22}	B_{33}	B_{12}	B_{13}	B_{23}
o-SrLiAs						
Sr	0.93(2)	0.73(2)	1.03(2)	0	−0.07(1)	0
As	0.94(2)	0.51(2)	0.85(2)	0	0.04(2)	0
h-SrLi$_{1-x}$As						
Sr	0.98(2)	B_{11}	0.98(3)	$^1/_2B_{11}$	0	0
As1	0.57(3)	B_{11}	0.68(3)	$^1/_2B_{11}$	0	0

[a]occ(Li) = 0.95(6), occ(As1) = 0.853(4), occ(As2) = 0.066(3).

The electron localizability indicator (ELI, γ) was evaluated in the ELI-D representation according to refs 19−21, using an ELI-D module within the program package TB-LMTO-ASA.[16] Topological analysis of the electron density, i.e., estimation of the shapes, volumes, and charges of the atoms after Bader (quantum theory of atoms in molecules, QTAIM),[22] and of the electron localizability indicator, e.g., localization of the ELI maxima as fingerprints of the direct atomic interactions, was performed with the program DGrid.[23]

3. RESULTS AND DISCUSSION

3.1. Composition and Thermal Behavior of *o*-SrLiAs and *h*-SrLi$_{1-x}$As Phases. Upon starting from the stoichiometric composition 1:1:1, a mixture of orthorhombic and hexagonal phases was obtained, which is probably the reason why these two phases were not recognized previously. With increasing amount of lithium in the starting mixture, more orthorhombic phase was obtained in the reaction product. Finally, the best starting ratio was found to be Sr:Li:As = 1:2:1, which resulted in single phase *o*-SrLiAs. The single-phase sample of hexagonal *h*-SrLi$_{1-x}$As was obtained by annealing *o*-SrLiAs at 550 °C for 2 h in an open tungsten crucible under a dynamic vacuum of 10^{-3} mbar.

The SrLiAs phases are unique in the series of equiatomic compounds in the systems {Ca, Sr, Ba, Eu, Yb}−Li−{As, Sb, Bi},[9] among which individual compounds crystallize in either the TiNiSi or the ZrBeSi structure type. In the Sr−Li−As system both atomic motifs coexist. The atomic arrangement is sensitive both to the amount of Li in the starting mixture and to the preparation temperature.

The preparation conditions indicate a formation of the orthorhombic and the hexagonal phase at slightly different compositions: *o*-SrLiAs was synthesized with a double amount of Li (Sr:Li:As = 1:2:1) in the starting mixture, while *h*-SrLi$_{1-x}$As was obtained by removing some Li from the orthorhombic phase under dynamic vacuum (cf. above). Reversibly, the hexagonal phase transforms back to the orthorhombic one when *h*-SrLi$_{1-x}$As was mixed with extra lithium and annealed in a closed Ta crucible at 800 °C.

The DSC study on an *o*-SrLiAs sample (Figure 1) reveals two sharp endothermic effects at 178 and 826 °C. The former peak corresponds to the melting of excess lithium (180.5 °C).[24]

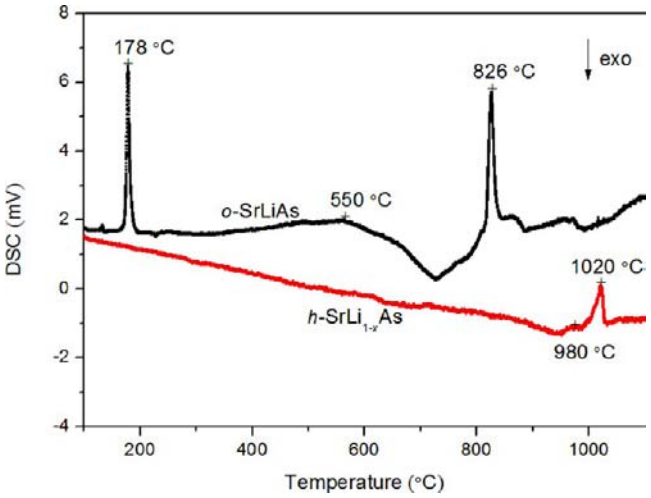

Figure 1. Thermal behavior of polycrystalline samples *o*-SrLiAs and *h*-SrLi$_{1-x}$As.

The latter one results from the (peritectic) decomposition of *o*-SrLiAs into *h*-SrLi$_{1-x}$As and melt, which is verified by powder X-ray diffraction pattern obtained on this sample after DSC measurement (Figure 2). The exothermic effect at 550 °C is

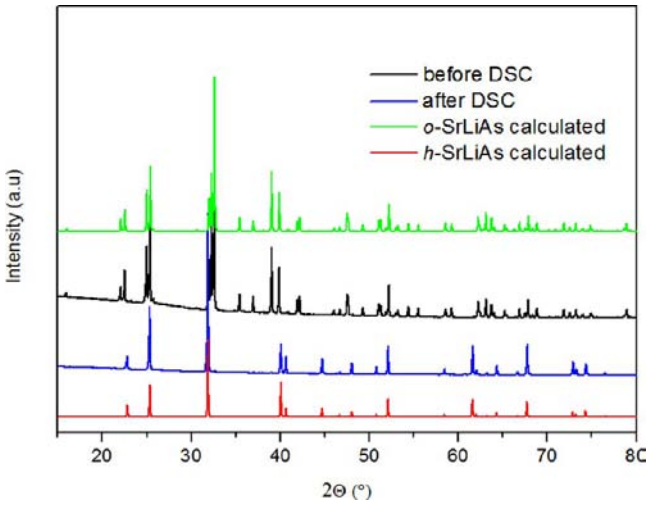

Figure 2. Powder X-ray diffraction patterns of *o*-SrLiAs sample before and after DSC measurement (Cu Kα_1 radiation). The calculated patterns are shown for comparison.

ascribed to the peritectoid decomposition of the orthorhombic phase. From these data, *o*-SrLiAs only exists in a limited temperature range between 550 and 826 °C.

By heating of a sample of *h*-SrLi$_{1-x}$As, two endothermic peaks around 1000 °C were observed (Figure 1). The signal at 980 °C corresponds to the (peritectic) decomposition of *h*-SrLi$_{1-x}$As; the peak at 1020 °C represents the liquidus temperature. For comparison, the TG-DSC measurement was also performed on *h*-SrLi$_{1-x}$As in an open BN crucible. An endothermic peak at ∼840 °C combined with a significant mass loss was observed, revealing the decomposition of *h*-SrLi$_{1-x}$As in an open environment and concomitant release of lithium. The powder X-ray diffraction patterns of the products after both DSC measurements were similar and indicated the presence of several phases. One of them was identified as the binary compound SrAs.[25]

dx.doi.org/10.1021/ic401166v | Inorg. Chem. 2013, 52, 8971−8978

The chemical analysis of the *o*-SrLiAs and *h*-$SrLi_{1-x}As$ samples after preparation revealed oxygen contents below the limit of detection (0.25 mass %). The microstructure of the sample prepared from the mixture with component ratio 1:2:1 by reaction at 950 °C and annealing at 800 °C (96 h) revealed then the majority phase *o*-SrLiAs (according to XRPD), together with minority phases (Figure 3). One of these phases

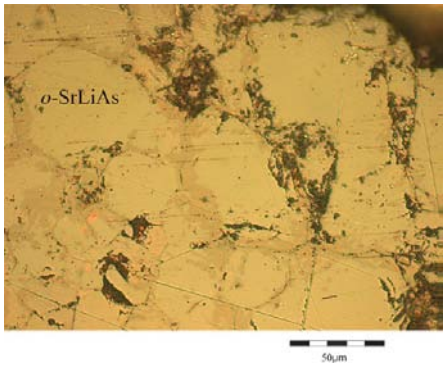

Figure 3. Microstructure of the SrLiAs sample. The majority phase *o*-SrLiAs as well as the minority phases can be recognized from the optical contrast.

may be *h*-$SrLi_{1-x}As$. Traces of an additional phase with the ratio Sr:As = 1:2 were also found. The ratio of Sr:As was found to be close to 1 in the majority phase according to the EDXS. No difference in the Sr:As ratio could be detected between *o*-SrLiAs and *h*-$SrLi_{1-x}As$ phases. The mass fractions of the elements in the majority phase are 51.58(17)%, 4.20%, and 44.22(17)% for Sr, Li, As, respectively (average from 10 points for Sr and As, WDXS analyzer). This yields the composition $Sr_{33.1}Li_{33.8}As_{33.1}$, which is in good agreement with the results of the crystal structure determination.

A sensitivity of the crystal structure to the (even slight) differences in composition is frequently observed in the ternary metallic systems. For instance, in the $EuGa_{2-x}Ge_x$ series two atomic arrangements were found.[26] For $x = 0.5$ the hexagonal AlB_2 type (aristotype to ZrBeSi) is observed, whereas $EuGa_2$ ($x = 0$) crystallizes in the KHg_2 type, which is closely related to the ternary TiNiSi type. Similar behavior was observed earlier in the $RENi_xGa_{2-x}$ systems (RE = rare earth metal), where upon increasing x the crystal structure changed from the AlB_2 prototype sequentially to the $CaIn_2$, KHg_2, and, finally, TiNiSi type observed at equiatomic composition ($x = 1$).[27]

3.2. Crystal Structure. The crystal structure of *o*-SrLiAs was solved within the space group *Pnma* using the single-crystal X-ray diffraction data by direct phase-determination technique.[28] The structure model was refined with anisotropic displacement parameters for Sr and As atoms, whereas the one for the Li position was kept isotropic.

An atomic arrangement of the structure type ZrBeSi (space group $P6_3/mmc$)[29] was used as initial model for the refinement of the *h*-$SrLi_{1-x}As$ crystal structure. With anisotropic displacement values of the Sr and the As positions, the refinement converged to R_F value of 0.028. This resulted in a significant anisotropy for the As position with a ratio $B_{33}/B_{11} \sim 2.5$, while the displacement for Sr position was roughly isotropic. This indicates that the As atoms prefer to be shifted from the ideal 2*c* position ($^1/_3$, $^2/_3$, $^1/_4$) along the [001] direction. The distribution of the difference electron density around the position ($^1/_3$, $^2/_3$, $^1/_4$) is shown in Figure 4. In the next step, As

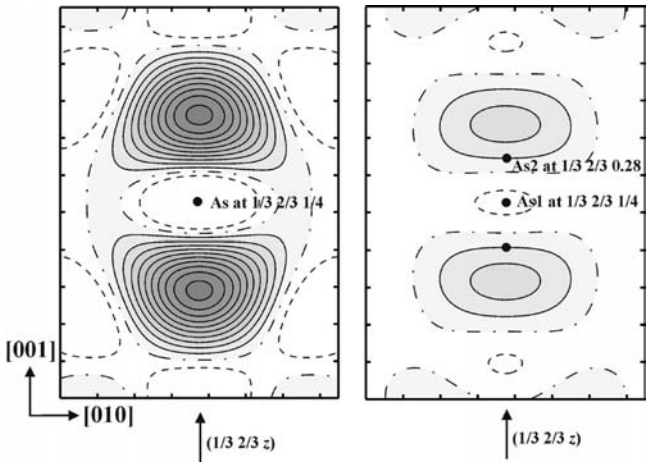

Figure 4. Residual electron density maps around the position $^1/_3$, $^2/_3$, $^1/_4$ in *h*-$SrLi_{1-x}As$: (left) with the As atoms positioned at $z = {}^1/_4$; (right) with the additional As atoms at $z \approx 0.28$. The isolines are shown in steps of 0.5 e/Å^3: solid line, positive values; dashed-dotted line, zero level; dashed lines, negative values.

atoms were located slightly away from the mirror plane into a 4*f* position with half occupancy. This yielded a residual density with a maximum at ($^1/_3$, $^2/_3$, $^1/_4$). The final refinement was made with As atoms at both 2*c* and 4*f* position at a ratio of 0.853(4):0.132(6). This made it also possible to refine the B_{iso} value and the occupancy parameter for the Li atom. The R_F value dropped slightly to 0.026. The value of occ(Li) = 0.95(6) is close to unity within one esd, but may suggest a possible defect at this position. All relevant information concerning data collecting and handling is listed in Table 2. Atomic coordinates, displacement parameters, and interatomic distances are presented in Tables 3 and 4.

Table 4. Selected Interatomic Distances (Å) for *o*-SrLiAs and *h*-$SrLi_{1-x}As$

o-SrLiAs		*h*-$SrLi_{1-x}As$	
atoms	distance	atoms	distance
Li–As (×2)	2.681(7)	Li–As1 (×3)[a]	2.5939(1)
Li–As (×1)	2.817(13)	Li–As2 (×3)[a]	2.606(3)
Li–As(×1)	2.928(13)	Sr–As2 (×6)[a]	3.143(5)
Sr–As(×1)	3.169(1)	Sr–As1 (×6)[a]	3.2903(1)
Sr–As (×2)	3.236(1)	Sr–Li (×6)	3.2903(1)
Sr–As (×2)	3.248(1)	Sr–As2 (×6)	3.449(6)
Sr–As (×1)	3.583(1)	Sr–Sr (×2)	4.0485(1)
Sr–Li (×2)	3.128(9)	Sr–Sr (×2)	4.4928(1)
Sr–Li (×1)	3.174(13)		
Sr–Li (×1)	3.494(13)		
Sr–Li (×2)	3.583(1)		
Sr–Sr (×2)	3.887(1)		
Sr–Sr (×2)	4.015(1)		

[a]The two Li–As distances are alternating distances. The two Sr–As distances are alternating distances.

The orthorhombic crystal structure of *o*-SrLiAs (Figure 5, top) belongs to the TiNiSi type, whereas the hexagonal structure pattern of *h*-$SrLi_{1-x}As$ is a disordered and distorted derivative of the ZrBeSi type (Figure 5, middle). In the nondistorted crystal structure of *h*-$SrLi_{1-x}As$ (As at 2*c* position), the alternating Li and As atoms form two-

dx.doi.org/10.1021/ic401166v | Inorg. Chem. 2013, 52, 8971–8978

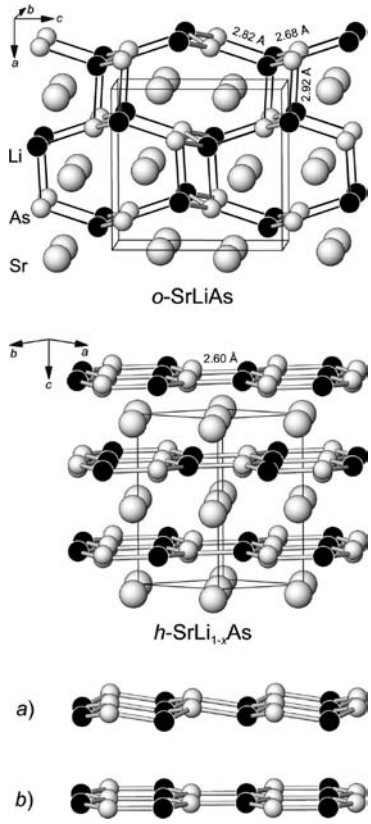

Figure 5. Crystal structures of *o*-SrLiAs (TiNiSi type) and *h*-$SrLi_{1-x}As$ (ZrBeSi type). Li and As atoms are connected such that they form 3D and quasi-2D frameworks, respectively. In the lower part of the figure two alternating Li–As frameworks in *h*-$SrLi_{1-x}As$ are shown: (a) corrugated with split As position (As2 at $z = 0.28$) and (b) planar with As atoms located at a mirror plane (As1 at $z = {}^1/_4$).

dimensional honeycomb layers at $z = {}^1/_4$ and $z = {}^3/_4$ with the Sr atoms embedded in-between. The appearance of an additional position for As atoms reflects their deviation from the mirror plane. This may be caused by bonding relations or may be the result of defects at the Li position. The distance Li–As within the planar layers is 2.594 Å; within the corrugated layers it amounts to 2.606 Å. Both values are very close to the Li–As contacts of 2.570 Å in binary Li_3As (Na_3As structure type).[30] The distance of 4.049 Å between adjacent Li–As layers is significantly larger, which suggests a 2D character of the Li–As substructure. Strontium atoms are sandwiched between two adjacent Li–As layers. Each Sr atom has 6 Li neighbors located at a distance of 3.290 Å. Sr–As distances range from 3.143 to 3.449 Å.

In the crystal structure of *o*-SrLiAs, each hexagon $[Li_3As_3]$ within the honeycomb layers is corrugated toward a chair configuration. This leads to the shortening of Li–As contacts between neighboring layers. Therefore, the Li–As substructure obtains topologically 3D character with distorted tetrahedral coordination of Li (As) atoms and Li–As distances of 2.681 (2×), 2.817, and 2.928 Å. These values are also comparable with the Li–As distance of 2.710 Å in LiAs.[31] The shorter Li–As contacts occur within the corrugated hexagons while the longer one is observed between the adjacent honeycomb layers. Sr atoms are located in cavities of the 3D Li–As framework. The Sr–Li and Sr–As distances cover larger intervals of 3.128–3.583 and 3.169–3.583 Å, respectively (Table 4).

A rather unexpected result is obtained from an analysis of the unit cell volumes of *o*-SrLiAs and *h*-$SrLi_{1-x}As$. Despite the defect on the lithium site, the hexagonal phase has larger volume per formula unit as the orthorhombic one. In a recent work on the TiGePt compound, similar behavior was explained by differences in the atomic interactions.[32] This assumption was the starting point for further quantum chemical studies of both title compounds.

3.3. Electronic Structure and Chemical Bonding. In order to understand the interplay between the electronic and crystal structures, the electronic density of states (DOS) was calculated for ordered model systems with complete occupation of all positions (Figure 6). Remarkably, the total DOS and its

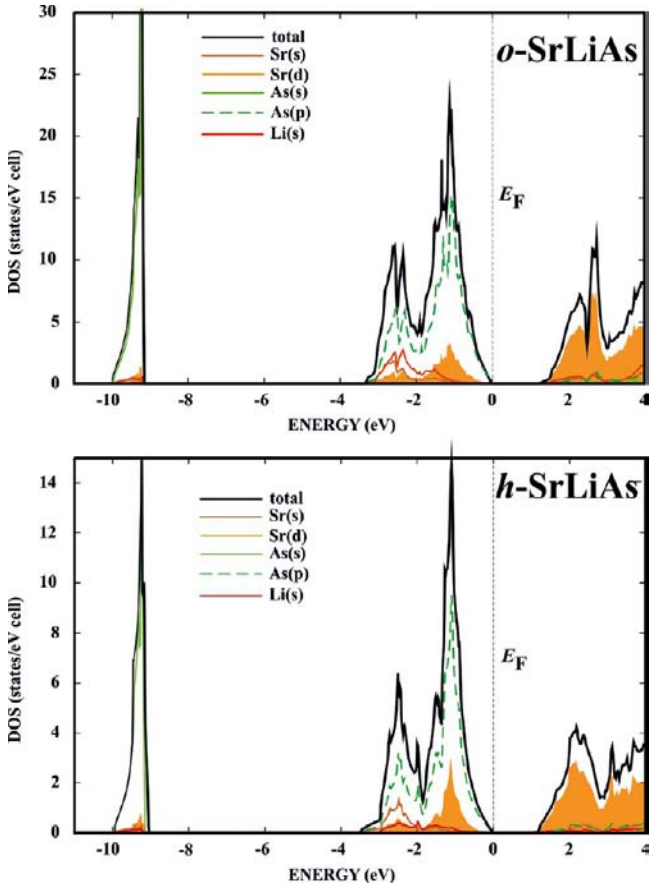

Figure 6. Calculated electronic density of states (DOS) for *o*-SrLiAs and *h*-SrLiAs.

partial atomic contributions are very similar for both compounds. The DOS below the Fermi level consists of two well separated regions. The low-energy range ($E < -9$ eV) is composed mainly of the As(s) states with minor participation of Li(s), Sr(s), Sr(d), and As(p) states which may indicate a rather lone-pair character of the As(s) states. This conclusion common to both crystal structures is in contradiction with the local environment of the As atoms in these structures: while they may be considered as three-bonded in the nondistorted structural pattern of *h*-$SrLi_{1-x}As$ (Figure 5, middle), the corrugation of honeycomb layers in the distorted ZrBeSi-type pattern and further in the TiNiSi-type pattern leads to the appearance of four-coordinated As species. Consequently, the bonding character of this part of the DOS is defined by the minor contributions of the metal s states. The DOS region just

dx.doi.org/10.1021/ic401166v | Inorg. Chem. 2013, 52, 8971–8978

below the Fermi level (-3.5 eV $< E < E_F$) is formed by the As(p) states mixed with Li(s), Sr(s), and Sr(d) contributions. For both compounds, the DOS reveals band gaps of approximately 1 eV above the Fermi level, and indicates semiconducting behavior assuming the ideal composition.

Further insight into the organization of the crystal structures was obtained by applying the analysis of atomic interactions in real space within the electron localizability approach.[23] From chemical intuition, the interaction between the Li−As framework and the embedded Sr atoms in both compounds may be expected as an ionic one. In such case the Sr atoms transfer their valence electrons to the framework in order to form covalent bonds. Because of the large electronegativity difference between lithium and arsenic, their presence in the same framework is not obvious at first glance. Thus, the atomic charges were calculated within the quantum theory of atoms in molecules (QTAIM)[22] for ordered models with full occupations of all positions in order to better understand the role of the different elements within the crystal structure. The shapes of the QTAIM atoms (atomic basins) in *o*-SrLiAs and *h*-SrLiAs are shown in Figure 7. Already the atomic basins of Sr have

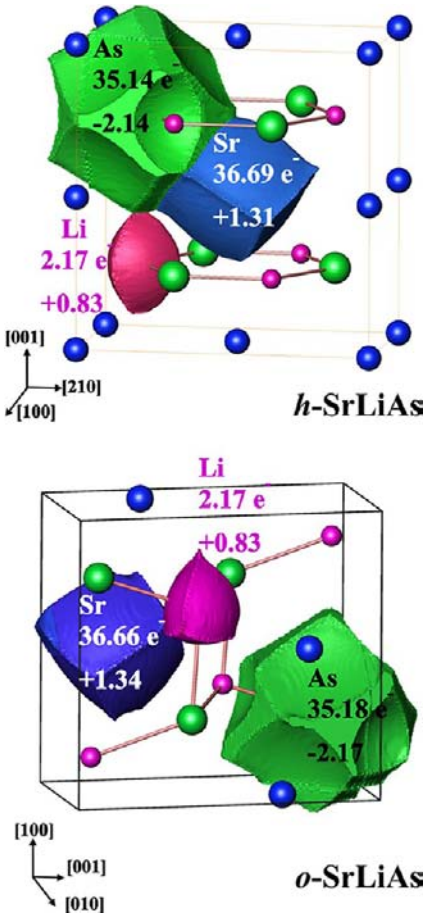

Figure 7. QTAIM atomic basins and effective charges for *o*-SrLiAs and *h*-SrLiAs.

shapes deviating markedly from a spherical one, which might be expected assuming their role as cations (cf., e.g., $Sr_8Al_6Si_{40}$[33]); the basins of As and Li resemble the tetrahedral or trigonal coordination of these atoms in the crystal structure having tetrahedron- or trigonal-bipyramid-like shapes in *o*-SrLiAs or *h*-SrLiAs, respectively. Despite the differences in the crystal structures, integration of the electron density within the atomic basins yields practically identical effective charges (Figure 7). In accordance with the electronegativities of the constituting elements, the strontium species carry the largest positive, and the arsenic, the largest negative charge, while the lithium shows an intermediate positive charge. The charge transfer is playing an important role in the organization of both crystal structures, *o*-SrLiAs and *h*-SrLiAs.

Analysis of the distribution of the electron localizability indicator in *o*-SrLiAs and *h*-SrLiAs reveals maxima of the ELI-D between As and Li (Figure 8, bottom) and confirms the direct covalent bonding within the Li−As framework. Despite the long Li−As contact between the adjacent honeycomb layers in *h*-SrLiAs, there are clear ELI-D attractors close to the As nucleus on this Li−As line, suggesting the transformation from a lone pair to a bonding character of the atomic interaction in this region of the crystal structure. Because this transformation is not complete, the nonbonding character dominates and the interlayer distance remains large and is responsible for the larger formula unit volume of the hexagonal phase. The ELI-D distribution in the penultimate shells of the Sr species slightly deviates from a spherical configuration in both compounds (Figure 8, top). The structuring in these shells, which may indicate a participation of electrons in these shells bonding in the valence region[20,34] (cf., DOS above), is stronger in *o*-SrLiAs. In both Sr−Li−As phases this feature is stronger as in the clathrate $Sr_8Al_6Si_{40}$[33] but much weaker than recently observed in the barium analogues $Ba_8Al_6Si_{40}$ and $Ba_8Au_6Ge_{40}$.[35] No ELI maxima were found between the Sr atom and the framework atoms, in contrast to the situation found, e.g., between Ba and Au in $Ba_8Au_6Ge_{40}$.[35] Thus, the atomic interactions in *o*-SrLiAs and *h*-SrLiAs can be summarized as follows: the frameworks are formed by covalent, polar Li−As bonds, and Coulomb interactions were found between the Sr cations and the framework.

3.4. Physical Properties. The magnetic susceptibility, $\chi(T)$, of polycrystalline specimens of *o*-SrLiAs and *h*-$SrLi_{1-x}As$ shown in (Figure 9, large symbols) depends weakly on the applied field $\mu_0 H$, indicating the presence of minor ferromagnetic impurities (equivalent to a few ppm of α-Fe). An extrapolation using the data at $\mu_0 H = 7$ and 3.5 T leads to corrected values of the susceptibility, $\chi_{corr}(T)$ (Figure 9, small symbols). A typical Curie-type contribution $\propto C/T$ (C = Curie constant) seen in $\chi_{corr}(T)$ at the lowest temperatures is due to small amount of paramagnetic impurities. The magnetic susceptibilities of the SrLiAs compounds can be described by the equation

$$\chi_{corr}(T) = \chi_0 + \chi_1 T + C/T$$

The intrinsic diamagnetic susceptibilities χ_0 at $T = 0$ are $-41(8) \times 10^{-6}$ emu mol^{-1} for *o*-SrLiAs and $-43(8) \times 10^{-6}$ emu mol^{-1} for *h*-$SrLi_{1-x}As$. The fitted values of C are equivalent to 0.03% and 0.05% of $S = {}^1/_2$ species, respectively, indicating polycrystalline materials with low defect concentrations. The rather strong intrinsic diamagnetic susceptibilities χ_0 indicate that both phases are nonmetallic, which is in agreement with the band structure calculations. No phase transitions are observed in magnetic susceptibility within the investigated field and temperature ranges.

dx.doi.org/10.1021/ic401166v | *Inorg. Chem.* 2013, 52, 8971−8978

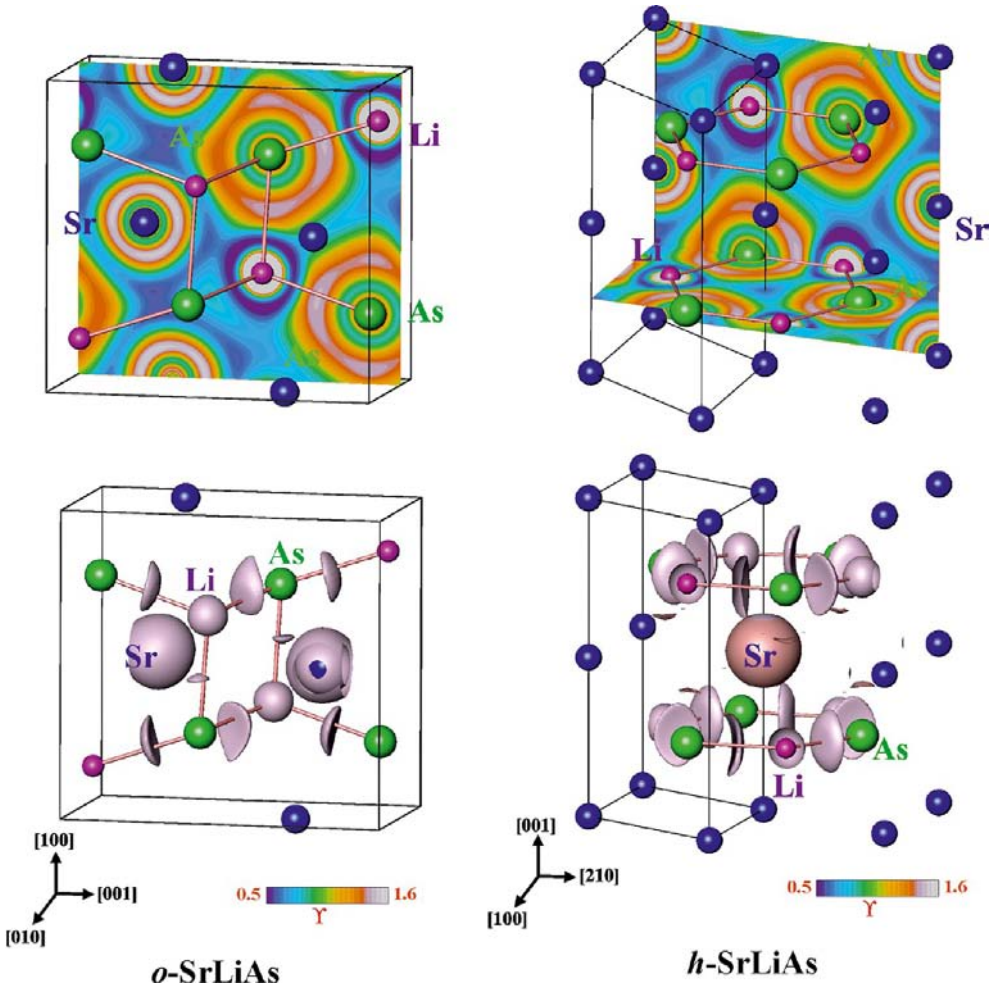

Figure 8. Electron localizability indicator in *o*-SrLiAs and *h*-SrLiAs.

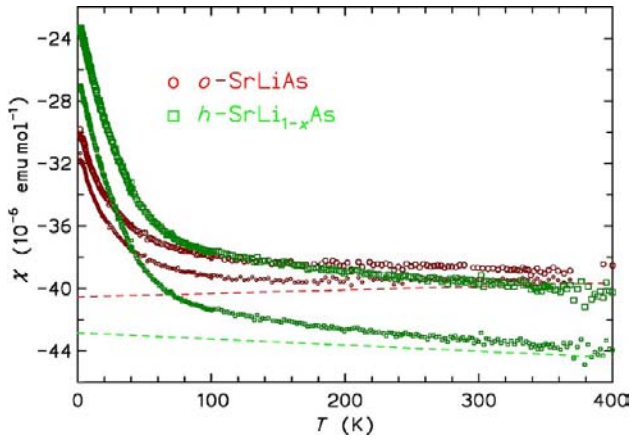

Figure 9. Molar magnetic susceptibility, $\chi(T)$, of polycrystalline *o*-SrLiAs and *h*-$SrLi_{1-x}As$ in a field of $\mu_0 H = 7$ T (large symbols). After correction for minor ferromagnetic impurities, the susceptibilities $\chi_{corr}(T)$ (small symbols) are obtained. The intrinsic susceptibilities for the two phases (obtained from the fit taking into account paramagnetic impurities) are shown by the dashed lines.

4. CONCLUSIONS

New Zintl phases, *o*-SrLiAs and *h*-$SrLi_{1-x}As$, were synthesized. Depending on the Li content, two structural patterns were identified: an orthorhombic TiNiSi type with stoichiometric amount of lithium, and a hexagonal ZrBeSi type with lithium deficiency. The orthorhombic *o*-SrLiAs transforms to *h*-$SrLi_{1-x}As$ at 550 °C in vacuum. Reversibly, *h*-$SrLi_{1-x}As$ partly turns back to *o*-SrLiAs by annealing with extra lithium. Analysis of the chemical bonding in real space shows that the framework in both phases is formed by covalent polar Li−As bonds, whereas Coulomb interactions were found between the Sr cations and the framework. Both phases of *o*-SrLiAs and *h*-$SrLi_{1-x}As$ are nonmetallic and diamagnetic, a finding which is in agreement with the calculated band structure and the analysis of chemical bonding.

■ ASSOCIATED CONTENT

Ⓢ Supporting Information

Crystallographic information files (CIF). This material is available free of charge via the Internet at http://pubs.acs.org.

■ AUTHOR INFORMATION

Corresponding Author

*E-mail: Juri.Grin@cpfs.mpg.de.

Author Contributions

The work was made in cooperation between two research groups. The manuscript was written based upon contributions from all authors. All authors have given approval to the final version of the manuscript.

dx.doi.org/10.1021/ic401166v | *Inorg. Chem.* 2013, 52, 8971−8978

Notes

The authors declare no competing financial interest.

■ ACKNOWLEDGMENTS

The authors are indebted to Dr. H. Borrmann and S. Hückmann for X-ray powder diffraction measurements and to Dr. F. R. Wagner for discussions on chemical bonding. We acknowledge Dr. G. Auffermann for chemical analysis, Mrs. S. Scharsach for thermal analyses, and Dr. S. Wirth, Dr. Y. Liang, and Dr. K. Guo for fruitful discussions. This research is in part supported by the CAS/SAFEA International Partnership Program for Creative Research Teams (Grant 51121064) and the MPG-CAS Partner Group Program.

■ REFERENCES

(1) Eisenmann, B.; Weiss, A.; Schäfer, H. *Z. Anorg. Allg. Chem.* **1972**, *391*, 241−254.
(2) Grund, I.; Zwiener, G.; Schuster, H. U. *Z. Anorg. Allg. Chem.* **1986**, *535*, 7−12.
(3) Merlo, F.; Pani, M.; Fornasini, M. L. *J. Less-Common Met.* **1990**, *166*, 319−327.
(4) Nesper, R. *Prog. Solid. State. Chem.* **1990**, *20*, 1−45.
(5) Prill, M.; Mosel, B. D.; Müller-Warmuth, W.; Albering, J.; Ebel, T.; Jeitschko, W. *Solid State Sci.* **2002**, *4*, 695−700.
(6) Eisenmann, B.; Liebrich, O.; Schäfer, H.; Weiss, A. *Z. Naturforsch.* **1969**, *B24*, 1344.
(7) Gupta, S.; Ganguli, A. K. *J. Solid State Chem.* **2006**, *179*, 1318−1322.
(8) Liebrich, O.; Schäfer, H.; Weiss, A. *Z. Naturforsch.* **1970**, *B25*, 650.
(9) Albering, J. H.; Ebel, T.; Jeitschko, W. *Z. Kristallogr. Suppl.* **1997**, *12*, 242.
(10) Feng, X.-J.; Prots, Yu.; Hoffmann, S.; Schnelle, W.; Zhao, J.-T.; Grin, Yu. *Book of Abstract*;13th European Conference of Solid State Chemistry, Lund, Sweden, September 25−28, 2011, p 81.
(11) Feng, X.-J.; Prots, Yu.; Schnelle, W.; Zhao, J.-T.; Grin, Yu. In preparation.
(12) *WinXPow, S., Version 2.08*; STOE & Cie GmbH: Darmstadt, Germany, 2003.
(13) Akselrud, L. G.; Zavalii, P.; Grin, Yu.; Pecharsky, V. K.; Baumgartner, B.; Wölfel, E. *Mater. Sci. Forum* **1993**, *133−136*, 335−340.
(14) Blessing, R. H. *Acta Crystallogr.* **1995**, *A51*, 33−38.
(15) Gelato, L. M.; Parthé, E. *J. Appl. Crystallogr.* **1987**, *20*, 139−143.
(16) Jepsen, O.; Burkhardt, A.; Andersen, O. K. *The Program TB-LMTO-ASA, 4.7*; Max-Planck-Institut für Festkörperforschung: Stuttgart, 1999.
(17) von Barth, U.; Hedin, L. *J. Phys. C* **1972**, *5*, 1629−1642.
(18) Andersen, O. K. *Phys. Rev. B: Condens. Matter Mater. Phys.* **1975**, *12*, 3060−3083.
(19) Kohout, M. *Int. J. Quantum Chem.* **2004**, *97*, 651−658.
(20) Wagner, F. R.; Bezugly, V.; Kohout, M.; Grin, Yu. *Chem.—Eur. J.* **2007**, *13*, 5724−5741.
(21) Kohout, M. *Faraday Discuss.* **2007**, 43−54.
(22) Bader, R. F. W. *Atoms in Molecules, A Quantum Theory*; Clarendon Press and Oxford University Press Inc: New York, 1994.
(23) Kohout, M. *DGrid, Version 4.6*, Radebeul, Germany, 2011.
(24) Lide, D. R. *Handbook of Chemistry and Physics*, 87th ed.; CRC Press: Boca Raton, FL, 2006.
(25) Iandelli, A.; Franceschi, E. *J. Less-Common Met.* **1973**, *30*, 211−216.
(26) You, T. S.; Zhao, J.-T.; Pöttgen, R.; Schnelle, W.; Burkhardt, U.; Grin, Yu.; Miller, G. J. *J. Solid State Chem.* **2009**, *182*, 2430−2442.
(27) Grin, Yu.; Yarmolyuk, Ya. P. *Izv. Akad. Nauk. SSSR, Met.* **1983**, 192−195.
(28) Altomare, A.; Cascarano, G.; Giacovazzo, C.; Guagliardi, A. *J. Appl. Crystallogr.* **1993**, *26*, 343−350.
(29) Nielsen, J. W.; Baenziger, N. C. *Acta Crystallogr.* **1954**, *7*, 132−133.
(30) Brauer, G.; Zintl, F. *Z. Phys. Chem.* **1937**, *B37*, 323−352.
(31) Cromer, D. T. *Acta Crystallogr.* **1959**, *12*, 36−41.
(32) Ackerbauer, S.-V.; Senyshyn, A.; Borrmann, H.; Burkhardt, U.; Ormeci, A.; Rosner, H.; Schnelle, W.; Gamza, M.; Gumeniuk, R.; Ramlau, R.; Bischoff, E.; Schuster, J. C.; Weitzer, F.; Leithe-Jasper, A.; Tjeng, L. H.; Grin, Yu. *Chem.—Eur. J.* **2012**, *18*, 6272−6283.
(33) Roudebush, J. H.; Tsujii, N.; Hurtando, A.; Hope, H.; Grin, Yu.; Kauzlarich, S. M. *Inorg. Chem.* **2012**, *51*, 4161−4169.
(34) Kohout, M.; Wagner, F. R.; Grin, Yu. *Theor. Chem. Acc.* **2002**, *108*, 150−156.
(35) Zhang, H.; Borrmann, H.; Oeschler, N.; Candolfi, C.; Schnelle, W.; Schmidt, M.; Burkhardt, U.; Baitinger, M.; Zhao, J.-T.; Grin, Yu. *Inorg. Chem.* **2011**, *50*, 1250−1257.